DesignCon2007
Leading Edge Communication Design Conference

A Generic and Higher Order Model For High-Speed Test Interface Analysis and De-embedding

Mike Li, PhD
Wavecrest Corporation

Abstract

It is well known that the output signals measured by a test/measurement system are not only due to the device-under-test (DUT), but also due to the test path or test interfaces. For example, if the intersymbol interference (ISI) due to the test path is not negligible, then the performance of the DUT can be grossly underestimated or overestimated, depending on whether it is an output test or input test. In this paper, we propose a generic model with extension to high orders for both the test path and the DUT. By using a cascading model, we will illustrate the measured signals due to the test path and DUT combined, in contrast to the measured signals due to the DUT alone. We will investigate both the effect of the limited bandwidth and the effect of ringing. We will illustrate the eye-diagrams of the DUT, and conceptually identify, separate, and de-embed the impact of the test path on the eye-diagrams, resulting in accurate measurement results and yield for the DUT.

Author Biography

Dr. Mike Li:

Dr. Mike Li is currently the Chief Technology Officer (CTO) with Wavecrest. Dr. Li pioneered jitter separation method (Tailfit) and DJ, RJ, and TJ concept and theory formation. He has been involved in setting and contributing to standards for jitter, noise and signal integrity for leading serial data communications such as Fibre Channel, Gigabit Ethernet, Serial ATA, PCI Express and FB DIMM. Currently, he is Co-Chairman for the PCI Express jitter standards committee. Dr. Li has been involved in technical committees for IEEE- and IEC-sponsored technical conferences such as International Test Conference (ITC) and DesignCon. He is an invited speaker, a panelist, session and panel chairs on the subjects of jitter/noise and signal integrity covering both design and test.

Dr. Li has more than 15 years experience in high-speed related measurement instrumentation, testing and analysis/modeling algorithms/tools, with applications in IC, microprocessor, clock, serial data communications for both electrical and optical, and wireless communication. Prior to joining Wavecrest, Dr. Li had worked in both industry and academic institution. Dr. Li is experienced in measurement system and Automated Test Equipment (ATE) architectures, hardware, software, performance, and accuracy. He has a BS in physics from University of Science and Technology of China, a MSE in electrical engineering and a Ph.D. in physics from University of Alabama in Huntsville. He did his Post Dr. at University of California, Berkeley and worked there as a research scientist on high-energy astrophysics before he joined industry. Dr Li has published more than 70 papers in refereed technical journals and conferences and one book on high-speed design and test, has filed 12 patents, with 4 granted and 8 pending.

1.) Introduction

For high-speed communication devices, signal integrity has become an increasingly important issue. In a typical test and measurement system, the measured signals are not only due to the device-under-test (DUT) that is of interest to us, but also due to the test path, i.e., signal generator, the cables/traces, test fixture/socket, etc[1]. With very tight performance requirements, the degradation of the signal integrity due to the test path rather than the DUT itself is no longer negligible, therefore, serious effort is required to isolate and measure the true performance of the DUT. For example, with a very tight jitter budget, we no longer have the luxury of measuring the jitter performance due to both the test path and the DUT and then reporting the results as the jitter performance of the DUT because many good DUTs will fail due to the excessive jitter introduced by the test path.

Several authors have addressed the issues of simulating and characterizing the test path[1],[2],[3], many times referred to as tester interface (TI) or device interface (DI). The modeling was generally limited to a single component along the test path while the characterization of the overall test path was mainly through measurement. A linear system response approach was recently presented to model the overall response for the test path to initiate the discussion on the effect of the limited frequency bandwidth [1], however, the effect of ringing was not addressed. Because it was mostly based on simple one-pole model, only timing errors through the step response analysis (rise/fall times) were illustrated.

In this paper, we propose a much more generic model for both the test interface and the DUT. By using a cascading model, the measured signals can be characterized as a convolution of the input signal, the impulse responses of the components along the test interface and the impulse response of the DUT. In the frequency domain, cascading is simply multiplying the transfer functions of each stage.

We will examine several higher order systems (the order of the system is determined by how many poles) with zeros and multiple poles. We will not only examine the magnitude response but also the phase response of the transfer function. The eye-diagrams will be presented to estimate not only the timing errors but also the amplitude errors. Finally, by allocating certain zeros and poles to the DUT, with all the rest allocated to the test interface and path, we can conceptually identify and separate the impact of the test path on the eye-diagrams. We will also investigate several different test patterns commonly used in communications, including the K28.5, PRBS and CJTPAT to examine the intersymbol interference (ISI) or data dependent jitter (DDJ).

For convenience, throughout this paper, we adopt the normalized time base, i.e., 1 unit interval (UI) based on the data communication bit rate, and therefore the normalized frequency unit is 1/UI. The peak-to-peak reference voltage is also normalized to be one.

2.) Theory

2.1 A Typical I/O Tester Setup:

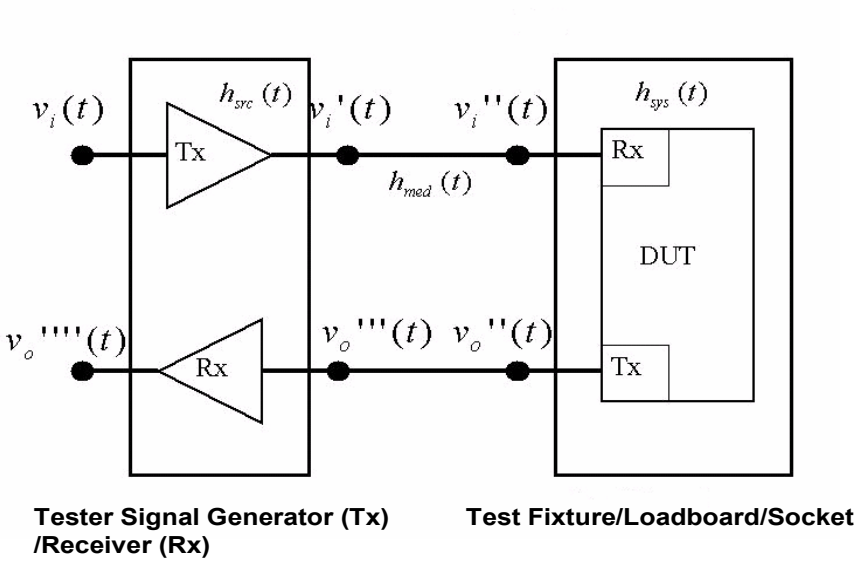

Fig. 1 shows a typical I/O tester setup for standard functional tests, where $v_i(t)$ is initial stimulus from the signal generator, and $v_o''''(t)$ represents the final test receiver measured signal. It is important to notice that there are several test points between the measurement system ports and the load board/DUT interface ports.

Consider an ideal case, i.e., the impact of the test path is negligible, then we can obtain,

$$v_i(t) \otimes h_{sys}(t) = v_o(t) \tag{1}$$

where $h_{sys}(t)$ denotes the impulse response of the DUT that is of interest to us, and $\otimes$ denotes a time domain convolution.

If we denote the impulse response of the tester signal generator as $h_{src}(t)$ and the impulse response of the media (can be connector, cable, tester fixture/socket lumped together) as $h_{med}(t)$, then we can write,

$$v_i(t) \otimes h_{src}(t) \otimes h_{med}(t) \otimes h_{sys}(t) = v_o''(t) \tag{2}$$

For simplicity, we consider $v_o''(t)$ rather than $v_o''''(t)$ as the measured signal to include only one pass of the impact of the test path. Clearly,

$$v_o(t) \otimes h_{src}(t) \otimes h_{med}(t) = v_o''(t) \tag{3}$$

and

$$v_i''(t) \otimes h_{sys}(t) = v_o''(t) \tag{4}$$

We therefore define the impulse response of the test path as,

$$h(t) = h_{src}(t) \otimes h_{med}(t) \tag{5}$$

If we adopt the bilateral Laplace transform to connect the time domain and the frequency domain, i.e.,

$$\begin{cases} H(s) = \int_{-\infty}^{\infty} h(t) e^{-st} dt, \quad ROC \\ h(t) = \dfrac{1}{2\pi j} \int_{\sigma - j\omega}^{\sigma + j\omega} H(s) e^{st} ds \end{cases} \tag{6}$$

where $s = \sigma + j\omega, j = \sqrt{-1}$ is complex, which defines the complex *S*-plane. The transfer function of the test path is,

$$H(s) = H_{src}(s) H_{med}(s) \tag{7}$$

2.2 A Generic Transfer Function Model:
Consider a linear time invariant (LTI) system that can be specified with constant coefficient linear differential equations. In *S*-plane, its transfer function can be represented in a rational form, i.e.,

$$\begin{aligned} \Psi(s) &= K \frac{s^M + a_{M-1} s^{M-1} + \cdots + a_0}{s^N + b_{N-1} s^{N-1} + \cdots + b_0} \\ &= K \frac{\prod_{m=1}^{M} (s + z_m)}{\prod_{n=1}^{N} (s - p_n)} \end{aligned} \tag{8}$$

where *N* and *M* denote the numbers of poles and zeros, respectively, and this is an N^{th}-order system.

Several observations can be made for this generic rational form representing the transfer function of a physically realizable system:

It must be causal, i.e., the region of convergence (*ROC*) is right to the rightmost pole[4];
It must be stable, i.e., all the poles are located in the left half of the *S*-plane (not including the imaginary axis), and the number of poles is greater than or equal to the number of zeros[4].

As a special example, if the number of poles is equal to the number of zeros, i.e., $N = M$, then we can rewrite Eq. (8) as,

$$\begin{aligned} \Psi(s) &= K \frac{s^N + a_{N-1} s^{N-1} + \cdots + a_0}{s^N + b_{N-1} s^{N-1} + \cdots + b_0} \\ &= K + K \frac{(a_{N-1} - b_{N-1}) s^{N-1} + \cdots + (a_0 - b_0)}{s^N + b_{N-1} s^{N-1} + \cdots + b_0} \end{aligned} \tag{9}$$

It is well known that the extra constant *K* in the frequency domain will induce a perfect Dirac delta function (as the impulse response) and a perfect step function (as the step response) in time domain.

However, this scenario is of little interest to us, and we will only consider the cases in which the number of poles is greater than the number of zeros.

For transfer functions that behave like a low-pass filter with fairly flat response in the pass band, we further limit that the poles and zeros cannot be located on or very close to the imaginary axis.

Assuming that $p_n \neq 0$ and $z_m \neq 0$, and the normalization constant K can be defined as,

$$K = \frac{b_0}{a_0} = \frac{\prod_{n=1}^{N}(-p_n)}{\prod_{m=1}^{M} z_m} \tag{10}$$

In a high-speed I/O test configuration, we can define this transfer function to be the transfer function due to both the test path and the DUT, i.e.,

$$\begin{aligned} \Psi(s) &= H(s)H_{sys}(s) \\ &= H_{src}(s)H_{med}(s)H_{sys}(s) \end{aligned} \tag{11}$$

The advantage of using such a formulation is that we can have a rational model with associated poles and zeros for each component along the test path, a rational model with associated poles and zeros for the DUT, and the combined transfer function (after multiplication) is still rational.

If we notice that each stage itself is a physically realizable system, it is reasonably safe to assume that we will have many more poles than zeros in the combined transfer function. For illustration purpose, we will only consider the transfer functions that only have poles (no zeros). They are the simplest and yet very representative.

2.3 A Generic De-embedding Method

According to Eq. (2), the true DUT output signal should be $v_{DUT}(t) = v_i(t) \otimes h_{sys}(t)$. The measured the output signal from the DUT is $v_o''(t)$, not $v_{DUT}(t)$. If the impulse response of the transfer functions for the signal generator $h_{src}(t)$ and interface media $h_{med}(t)$ are known, then their effects to the measurement results can be removed or de-embedded according to the inverse form of Eq. (2), namely:

$$v_{DUT}(t) = v_o''(t) \otimes^{-1} h_{src}(t) \otimes^{-1} h_{med}(t) \tag{12}$$

Where $\otimes^{-1}$ denotes the deconvolution operation. In frequency-domain, Eq. (12) can be rewritten as:

$$V_{DUT}(s) = \frac{V_o''(s)}{H_{src}(s)H_{med}(s)} \tag{13}$$

Eq. (12) and (13) defines a generic test interface de-embedding method.

3.) Model Building Blocks

In this section, we will review several fundamental rational models that will be considered as "building blocks". We will examine their magnitude/phase responses in frequency domain and their impulse/step responses in time domain.

We will focus on the denominator of the rational model shown in Eq. (8). There are typically two scenarios that we must consider:

If there is single pole, then it must be real and negative, and we have a factor of $(s - p_n)$ in the denominator (the 1st-order model);

If there are complex poles, then they must come as a complex conjugate pair, and we have a factor of $(s - p_n)(s - p_n^*) = s^2 + 2\zeta\omega_n s + \omega_n^2$ in the denominator, where * denoted complex conjugate, ω_n is the natural frequency and ζ is the damping ratio or factor (the 2nd-order model).

Therefore we choose these 1st-order and 2nd-order models as our basic "building blocks" for the model consideration.

3.1 The 1st-order Rational Model

This is the classic text-book model that was the focus and base of many previous papers[1], [2], [3].
Consider a one-pole rational model, i.e.,

$$\begin{aligned} \Psi(j\omega) &= K\frac{1}{j\omega - p_n}, \qquad \text{ROC} \\ &\Updownarrow \\ \psi(t) &= Ke^{p_n t}, \qquad t \geq 0 \\ \gamma(t) &= \frac{K}{-p_n}(1 - e^{p_n t}), \qquad t \geq 0 \end{aligned} \tag{14}$$

where $\psi(t)$ and $\gamma(t)$ denote the impulse and step responses, respectively, and $K = -p_n$.

Following the classical *RC* implementation of this transfer function, the time constant can be written as $\tau = \frac{1}{(-p_n)}$. The 3 dB cutoff frequency can be written as,

$$f_{3dB} = \frac{1}{2\pi\tau} = -\frac{p_n}{2\pi} \tag{15}$$

and the break frequency is at $2\pi f_{3dB}$. Beyond this frequency, the magnitude response follows the "20 dB per decade" asymptote. The "rule of thumb" for the rise time is [1] [2]:

$$\begin{cases} tr_{10-90\%} = \dfrac{\ln(9)}{f_{3dB}} = \dfrac{0.35}{f_{3dB}} \\ tr_{20-80\%} = \dfrac{\ln(4)}{f_{3dB}} = \dfrac{0.22}{f_{3dB}} \end{cases} \tag{16}$$

We have chosen $p_n = -5$. Fig. 1 shows the frequency domain magnitude and phase responses (Bode plot), while Fig. 2 shows the time domain impulse and step responses, respectively.

With the 3-dB cutoff frequency at 0.80, the rise times 10-90% of 0.44 and 20-80% of 0.28 obtained in the simulation (shown in Fig. 2) agree with those can be obtained by the "rule of thumb"[1], [2].

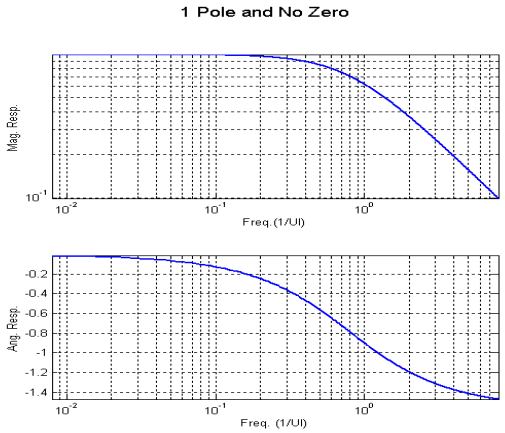

Figure 1. A one-pole model: Magnitude and phase responses in frequency domain.

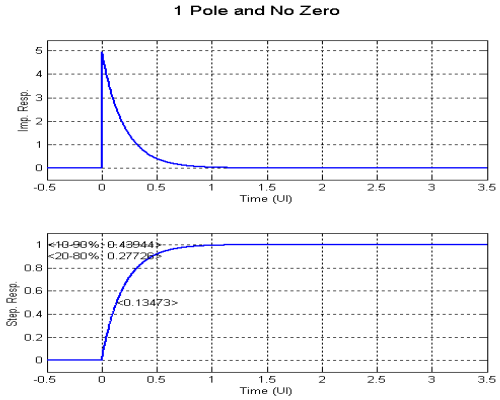

Figure 2. A one-pole model: Impulse and step responses in time domain.

3.2 The 2nd-order Rational Model

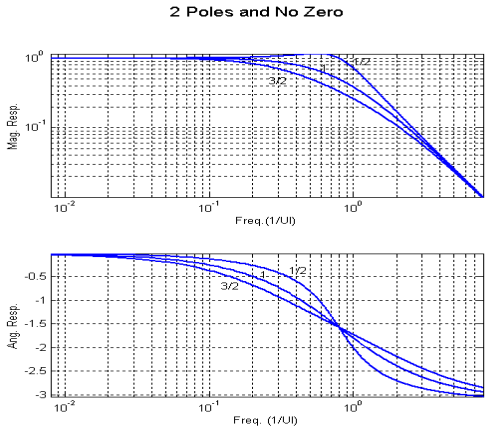

Figure 3. A two-pole model (under damped, critically damped and over damped cases): Magnitude and phase responses in frequency domain

This is a model of great interest because it starts to shed a lot of insight of the complexity of a real physical system.

Consider a two-pole rational model, i.e.,

$$\begin{aligned}
&\Psi(j\omega)=\frac{K}{(j\omega-p_n)(j\omega-p_k)}, ROC\\
&\Updownarrow\\
&p_n\neq p_k,\\
&\psi(t)=KA\left(e^{p_nt}-e^{p_kt}\right), \quad t\geq 0\\
&\gamma(t)=-KA\left(\frac{1-e^{p_nt}}{p_n}-\frac{1-e^{p_kt}}{p_k}\right), \quad t\geq 0\\
&p_n=p_k=\omega_n,\\
&\psi(t)=Kte^{p_nt}, \quad t\geq 0\\
&\gamma(t)=1-e^{p_nt}+p_nte^{p_nt}, \quad t\geq 0
\end{aligned} \tag{17}$$

where $\psi(t)$ and $\gamma(t)$ denote the impulse and step responses, respectively. $K = p_n p_k$ and $A=\frac{1}{p_n-p_k}$. Following the classical *RLC* implementation of this transfer function, the undamped natural frequency can be written as $\omega_n=\sqrt{p_n p_k}$ and the damping ratio can be written as $\zeta=-\frac{p_n+p_k}{\omega_n}$. We can also define the quality factor as $Q=\frac{1}{2\zeta}$. It is important to notice that the 3 dB cutoff frequencies are dependent on the damping ratio, while the break frequency is at ω_n, which is independent of the damping ratio. Beyond this frequency, the magnitude response follows the "40 dB per decade" asymptote. If we can break the 2nd-order model into two stages of cascading 1st-order model, then we have the "rule of thumb" based on the rise time of each stage (as a 1st-order model). If we denote the two cascading stages as *n* and *k*, then the "rule of thumb" for the rise time is [1],[2]:

$$tr_{nk}=\sqrt{tr_n^2+tr_k^2} \tag{16}$$

This rise time estimation is applicable to both the 10-90% rise time and the 20-80% rise time. On the other hand, if we cannot break the 2nd-order model into two stages of cascading 1st-order model, then there is no known simple 'rule of thumb" for the rise time.

We can choose $\zeta=\frac{1}{2}$ and $\omega_n=5$ ($p_n=\frac{5}{2}(-1+j\sqrt{3})$ and $p_k=\frac{5}{2}(-1-j\sqrt{3})$) for the under damped case; $\zeta=1$ and $\omega_n=5$ ($p_n=p_k=-5$) for the critically damped case; and

$\zeta = \frac{3}{2}$ and $\omega_n = 5$ ($p_n = \frac{5}{2}(-3+\sqrt{5})$ and $p_k = \frac{5}{2}(-3-\sqrt{5})$) for the over damped case. Fig. 3 shows the frequency domain magnitude and phase responses (Bode plot), while Figures 4, 5, and 6 shows the time domain impulse and step responses for the three different cases, respectively.

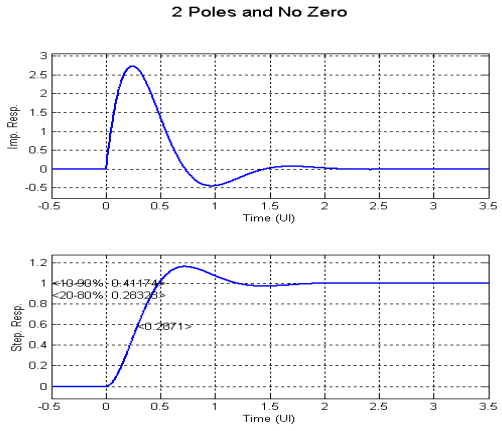

Figure 4. An under damped two-pole model: Impulse and step responses in time domain.

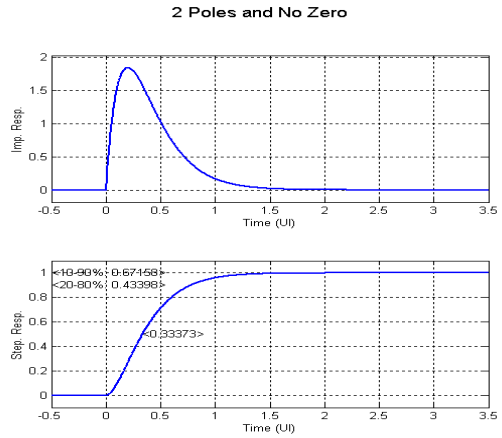

Figure 5. A critically damped two-pole model: Impulse and step responses in time domain.

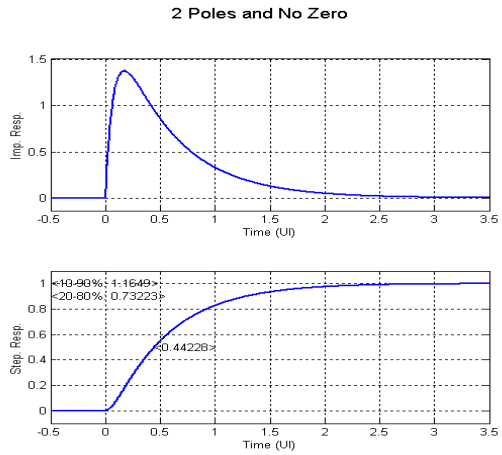

Figure 6. An over damped two-pole model: Impulse and step responses in time domain.

For the under damped case, clearly, $p_k = p_n^*$. The two poles are inseparable, i.e., it cannot be treated as two cascading stages of 1st-order model. This type of coupling is essential to the ringing (over-shoot, under-shoot) behaviors that we have observed. The rise times 10-90% of 0.41 and 20-80% of 0.28 obtained in the simulation (shown in Fig. 4) cannot be obtained by the "rule of thumb"[1],[2]. Therefore, this case represents a true 2nd-order "building block". For the rest of this paper, we shall consider only the true complex conjugate pair of poles for the 2nd-order model.

For the critically damped and over damped cases, it is clear that the poles are actually real, whether they are equal or not. These cases can be treated as cascading two 1st-order rational models; therefore it is the 1st-order model that constitutes the "building blocks" here. The rise times 10-90% of 0.67 and 20-80% of 0.43 obtained in the simulation for the critically damped case (shown in Fig. 5) and the rise times 10-90% of 1.16 and 20-80% of 0.73 obtained in the simulation for the over damped case (shown in Fig. 6) agree with those can be obtained by the "rule of thumb" [1],[2] .

Table 1. Rise time estimations for basic "building blocks"

	1st-order Model		2nd-order Model					
			Under Damped		Critically Damped		Over Damped	
	Numerical Estimation	"Rule of Thumb"	Numerical Estimation	"Rule of Thumb"	Numerical Estimation	"Rule of Thumb"	Numerical Estimation	"Rule of Thumb"
Rise Time (UI) 10-90%	0.44	0.44	0.41	N/A	0.67	0.67	1.16	1.16
Rise Time (UI) 20-80%	0.28	0.28	0.28	N/A	0.43	0.43	0.73	0.73

Table 1 summarizes the rise time estimations associate with "the building blocks". We have investigated two basic "building blocks": the 1st-order model and the true 2nd-order model (the under damped case). Their numerical examples of have very similar rise times. We will treat the test path using one of these two models: the 1st-order model can be used to illustrate the effect of the limited bandwidth, while the 2nd order model can be used to illustrate the effect of ringing.

4.) Simulation Experimental Results

In this section, we will examine a 2nd-order case and a 3rd order case that can be broken into lower order "building blocks". We will examine the eye-diagrams for these cases

Our goals are: (1) To illustrated that these models can be represented using the building blocks presented in the previous section; (2) If we allocate certain poles and zeros to the transfer function of the DUT that is of interested to us, we can illustrate the impact of the test path on the eye-diagrams by allocating all the other poles and zeros to the transfer function of the test interface path.

4.1 The DUT

For simplicity, we will assume that the DUT can be characterized as a 1st-order model, i.e., a one-pole low-pass filter.

Following the discussion on the 1st-order model in the previous section, we shall adopt the numerical results in Fig. 2 to characterize the DUT, and the corresponding eye-diagram is illustrated in Fig. 7. We observe very minimum timing and amplitude jitter. This will serve as a benchmark (the baseline) to illustrate the extra jitter and eye closure caused by the test path rather than the DUT alone.

The eye-diagrams presented here are all using the K28.5 bit pattern. The input data pattern is assumed to be ideal; i.e., the rise and fall times in the input data pattern are zero. We will consider different bit patterns in the next section.

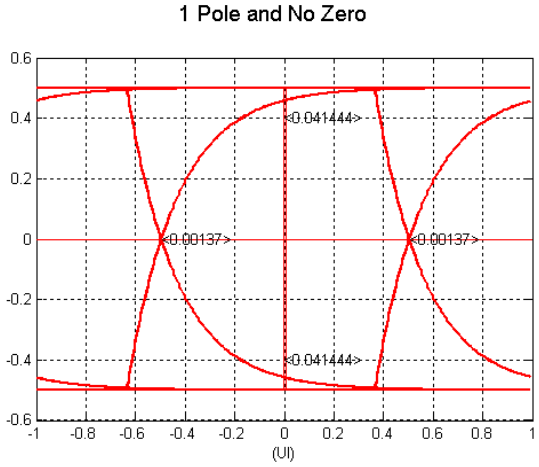

Figure 7. A one-pole model: Eye-diagram.

4.2 Test Path Impact: Limited Bandwidth

For the purpose of examining the effect of the limited bandwidth, we can model the test path as a one-pole low-pass filter.

We choose the first case such that the bandwidth of the test path is less than that of the DUT. The pole is located at $p_k = -3.75$. Fig 8 shows the combined eye-diagram due to both the test path and the DUT. We observed significant eye closure. The timing jitter increased by more than ten fold and the amplitude jitter more than doubled.

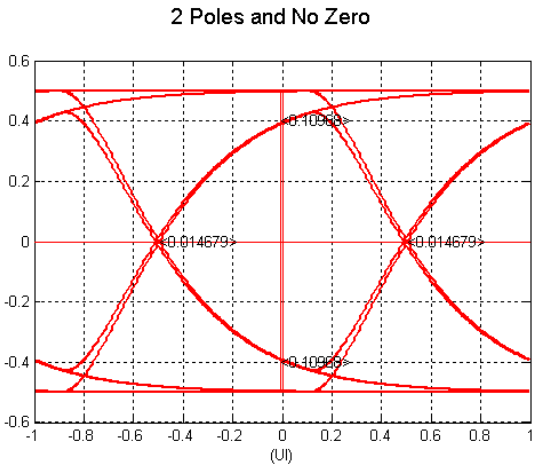

Figure 8. The combined eye-diagram: Test path as a one-pole low-pass filter

Now we choose the second case such that the bandwidth of the test path is greater than that of the DUT. The pole is located at $p_k = -6.25$. Fig 9 shows the combined eye-diagram due to both the test path and the DUT. We observed slight eye closure, which is in line with the slight increase of both timing and amplitude jitter.

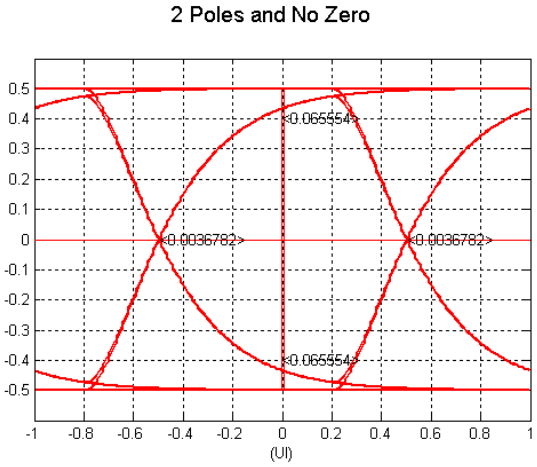

Figure 9. The combined eye-diagram: Test path as a one-pole, low-pass filter

This example serves to illustrate the effect of limited bandwidth of the test path. One of the fundamental design requirements is that the test path should have sufficient bandwidth to accommodate the intended DUTs. In both cases, we observed non-negligible timing and voltage ISI due to the test path rather than the DUT, therefore, the identification and separation of the test path impact is of critical importance in these cases.

4.3 Test Path Impact: Ringing

It is known from the previous section that we have to use the 2nd-order model in order to introduce the ringing behaviors. We can model the test path as a two-pole low-pass filter.

We choose a case such that $Q = 1$. The poles are located at: $p_k = \frac{5}{2}(-1 + j\sqrt{3})$ and $p_k^* = \frac{5}{2}(-1 - j\sqrt{3})$. Fig 10 shows the combined eye-diagram due to both the test path and the DUT. The timing and amplitude jitters are estimated to be 0.0013 and 0.094, respectively.

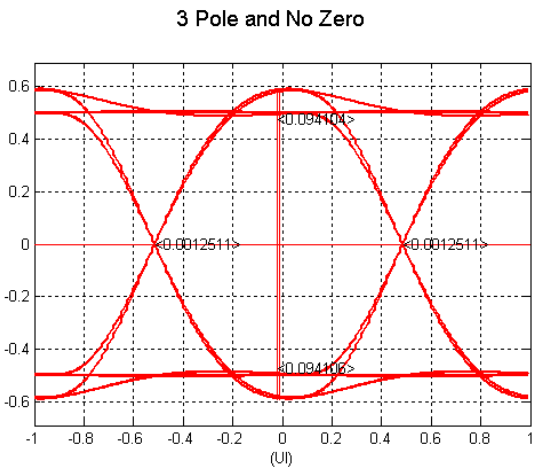

Figure 10. The combined eye-diagram: Test path as a two-pole, low-pass filter.

This example serves to illustrate the impact of the test path ringing. In this case, the ringing is small enough so that it does not clearly impact the 50% cross points, we observed increase of the amplitude ISI, but relatively small change of the timing ISI.

Table 2 summarizes the ISI estimations due to the DUT and the test path. In fact the last case demonstrated a reduced timing ISI, which actually hinted the principle of the compensation circuitry.

Table 2. K28.5 pattern ISI estimations due to DUT and test path

	DUT (Benchmark)	Effect of Limited Bandwidth				Effect of Ringing	
		Smaller Test Path Bandwidth		Larger Test Path Bandwidth			
		Combined	Test Path Induced	Combined	Test Path Induced	Combined	Test Path Induced
Timing ISI (UI)	0.0014	0.015	0.014	0.0037	0.0023	0.0013	-0.001
Voltage ISI	0.041	0.11	0.11	0.066	0.025	0.095	0.07

4.4 Test Path Impact De-embedding

As we have introduced, the path interface effect can be de-embedded via Eq. (12) in time-domain. For a de-convolution method, we refer readers to [5] and references therein. We consider the interface path impulse response is defined by a two-pole model described in 4.3. Its impulse response function is given by Eq. (17). Here we assume that the signal generator is ideal. The de-embedding will yields the following results:

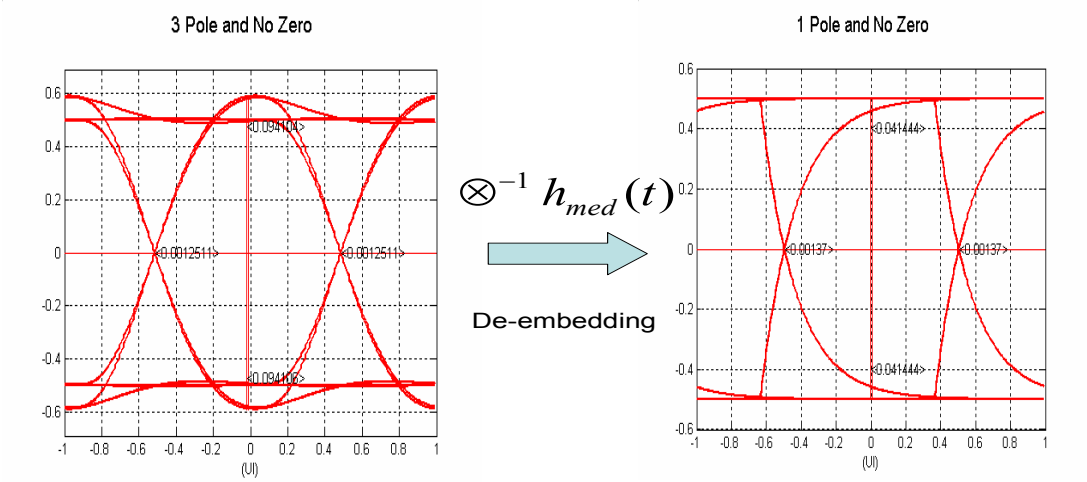

Figure 11. Test interface De-embedding illustration. After de-embedding, the eye-diagram becomes baseline of figure 7 from figure 10 where a two-pole interface effect is included.

The effects of test interface are clearly removed after de-bedding, leaving the true eye-diagram due to the DUT.

5.) Discussion

Consider an LTI system. It is apparent that there are three factors that will affect the output data ISI: (1) Input data pattern zero/one run length (the source), (2) system impulse/step response rise/fall time (the system bandwidth), and (3) the settling time of the system impulse/step response (due to the system's stability or instability, not applicable to the 1st-order rational model).

If there is no zero/one run length variation, e.g., in a Clock, there is only one zero/one run length, i.e., 1, we may only observe duty cycle distortion (DCD), but no ISI at all. Typically, the rise/fall times are predominantly determined by the system bandwidth. For a certain data rate, the rule of thumb is that the system bandwidth should be at least 0.75-0.78 of the inverse of the UI, in order to avoid excessively slow rise/fall times. If the rise/fall time is shorter than 1 UI, it is fairly safe to say that the rise/fall time does not cause any ISI; if the rise/fall time is longer than 1 UI, then it will start to contribute to the ISI caused by relatively shorter zero/one length in a data pattern. If the system has a fairly long settling time (more than 2-3 UIs), then we will see the ISI caused by the longer zero/one run length in the data pattern.

In short, we can define a system memory length to be the time from the start of the impulse/step response to the end when the impulse/step response fully settles. Clearly, both rise time and settling time contribute the system memory length. One example is that, if the system has a memory length of 2 UIs, then we will never see the ISI caused by zero/one run length beyond two UIs.

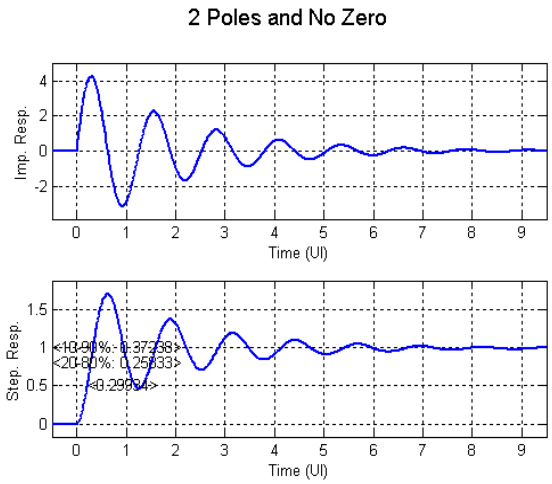

Figure 12. Test path as a two-pole, low-pass filter.

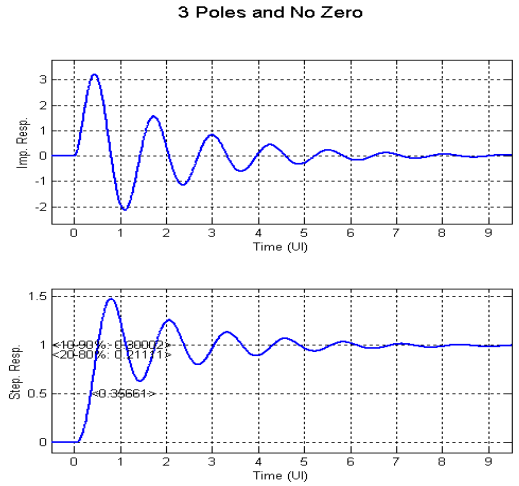

Figure 13. The combined eye-diagram: Test path as a three-pole, low-pass filter.

By examining the impulse/step response shown in previous sections, it is clear that their memory length is only around 2 UIs, i.e., the responses pretty much settle after two UIs. We would like to increase the system memory length and study the eye diagrams for three data patterns: K28.5 with zero/one run length up to 5, PRBS 2^{10}-1 with zero/one run length up to 10, and CJTPAT with zero/one run length up to 5. If we would like to maintain sufficient bandwidth, then we have to adopt to increase the settling time.

Consider now the test path as a two-pole low pass filter. This time we choose $Q = 5$ in order to increase the settling time, hence to increase the system memory length. The purpose is to evaluate the ISI due to much longer zero/one run length, e.g., up to 10. The poles are located at: $p_k = \frac{1}{2}(-1 + j3\sqrt{11})$ and $p_k^* = \frac{1}{2}(-1 - j3\sqrt{11})$.

Figures 14-16 show the combined eye-diagram due to both the test path and the DUT for three different data patterns. Respectively; for the K28.5 pattern, the timing and voltage jitters are estimated to be 0.14 UI and 0.86, respectively; for the PRBS 2^{10}-1 pattern, the timing and voltage jitters are estimated to be

0.26 UI and 0.91, respectively; and for the CJTPAT pattern, the timing and voltage jitters are estimated to be 0.26 UI and 0.91, respectively;

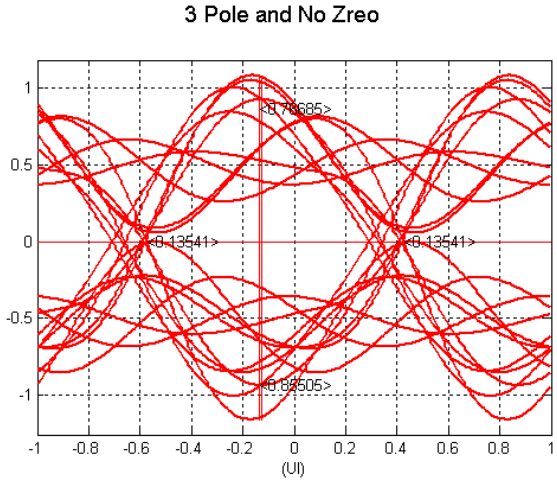

Figure 14. The combined eye-diagram for K28.5: Test path as a two-pole, low-pass filter.

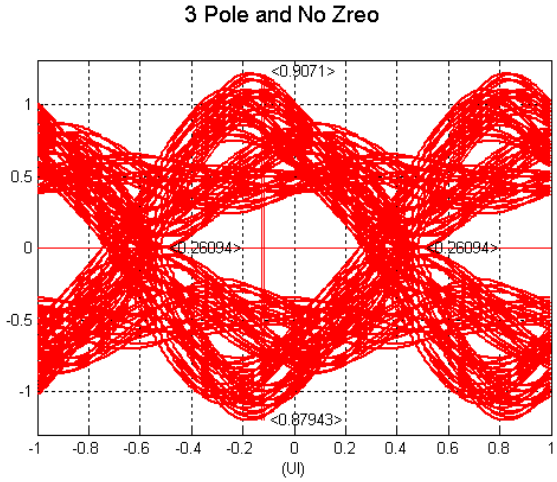

Figure 15. The combined eye-diagram for PRBS $2^{10}-1$: Test path as a two-pole, low-pass filter.

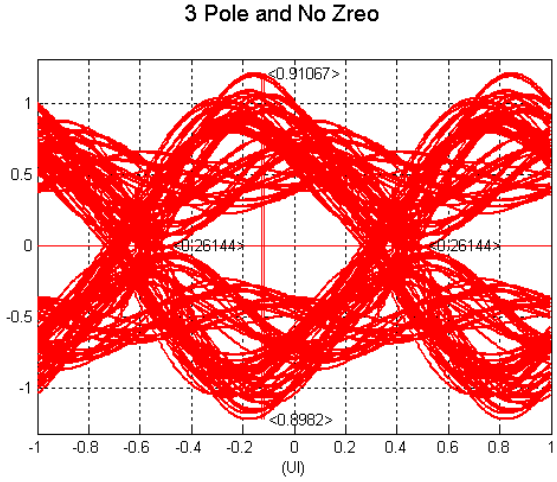

Figure 16. The combined eye-diagram for CJTPAT: Test path as a two-pole, low-pass filter

6.) Conclusion

We have illustrated a more generic model with scalable to higher orders for the high-speed test interface path and DUT. We demonstrated two basic "zeros" and "poles" based "building blocks", one is a 1st-order model (one-pole), the other is an under damped 2nd-order model (two-pole).

We not only investigated the effect of the limited bandwidth based on the 1st-order model; we also investigated the effect of ringing based on the 2nd-order model. Certain features not covered by a 1st-order model such as ringing is discussed

We examined signal eye-diagrams due to both the test path and the DUT for several different data patterns, and pointed out that the system memory length can significantly impact both the timing ISI and voltage ISI.

We illustrated a method for removing or de-embedding the effects of the test interface path to the DUT signal via deconvolution. This method can be adopted to fulfill the test interface de-embedding requirements imposed by some of the latest high-speed I/O test, such as PCI Express and FB DIMM.

REFERENCE

[1] Shimanouchi M., "New paradigm for signal path in ATE pin electronics are needed for serialcom device testing," ITC International Test Conference 2002 Proceedings, pages 903-912.

[2] Helmreich K., "Test path simulation and characterization," ITC International Test Conference 2001 Proceedings, pages 415-423.

[3] Schoettmer U., Wagner C. and Bleakley T., "Device Interfacing: The weakest link in the chain to break into the giga bit domain?" ITC International Test Conference 2000 Proceedings, pages 995-1004.

[4] Oppenheim A. V., Willsky A. S. and Young I., *Signals and Systems,* Chapter 4 and 9, 1983, Prentice-Hall, Inc., Englewood Cliffs, New Jersey.

[5] Sun J., Li M. and Wilstrup J., "A Demonstration of Deterministic Jitter Deconvolution", IMTC/IEEE, 2002.

FOR MORE INFORMATION CONTACT:

WAVECREST CORPORATION
7610 EXECUTIVE DRIVE
EDEN PRAIRIE, MN 55344
WWW.WAVECREST.COM
1(952)-646-0111